Enhancing the Efficiency of SnS Solar Cells bia Band-Offset Engineering with a Zinc Oxysulfide Buffer Layer

Enhancing the Efficiency of SnS Solar Cells via Band-Offset Engineering with a Zinc Oxysulfide Buffer Layer

Prasert Sinsermsuksakul,[1] Katy Hartman,[2] Sang Bok Kim,[1] Jaeyeong Heo,[1,a)] Leizhi Sun,[1] Helen Hejin Park,[1] Rupak Chakraborty,[2] Tonio Buonassisi,[2] and Roy G. Gordon[1,b)]

[1] *Harvard University, Cambridge, Massachusetts 02138, USA*

[2] *Massachusetts Institute of Technology, Cambridge, Massachusetts 02139, USA*

Abstract

SnS is a promising Earth-abundant material for photovoltaic applications. Heterojuction solar cells were made by vapor deposition of *p*–type tin(II) sulfide, SnS, and *n*-type zinc oxysulfide, Zn(O,S), using a device structure of soda-lime glass/Mo/SnS/Zn(O,S)/ZnO/ITO. A record efficiency was achieved for SnS-based thin-film solar cells by varying the oxygen-to-sulfur ratio in Zn(O,S). Increasing the sulfur content in Zn(O,S) raises the conduction band offset between Zn(O,S) and SnS to an optimum slightly positive value. A record SnS/Zn(O,S) solar cell with a S/Zn ratio of 0.37 exhibits short circuit current density (J_{sc}), open circuit voltage (V_{oc}) and fill factor (FF) of 19.4 mA/cm^2, 0.244 V and 42.97%, respectively, as well as an NREL-certified total-area power-conversion efficiency of 2.04% and an uncertified active-area efficiency of 2.46%.

[a] Curent address: Department of Material Science and Engineering, Chonnam National University, Gwangju 500-757, South Korea.

[b)] Author to whom correspondence should be addressed. Electronic mail: gordon@chemistry.harvard.edu

The toxicity of Cd and the scarcity of Te, In, and Ga used in CdTe and Cu(In,Ga)S_2 (CIGS) thin-film solar cells have motivated a search for alternative non-toxic, Earth-abundant, and inexpensive materials.[1] Tin(II) sulfide (SnS) is among the ongoing investigated materials such as Cu_2O,[2] Cu_2S,[3] FeS_2,[4,5] $Cu_2ZnSn(S_xSe_{1-x})_4$,[6] and $ZnSnP_2$.[7] SnS has a suitable bandgap (E_g ~ 1.1 - 1.5 eV),[8,9] strong optical absorption ($\alpha > 10^4$ cm^{-1}),[10] and proper carrier concentration ([p] ~ 10^{14} - 10^{17} cm^{-3}).[11] Recently, a record efficiency SnS solar cell of 1.95% (active area) was fabricated from *p*-*n* homojunction nanowires using boron and phosphorus as dopants.[12] In addition, SnS-based solar cells have been reported using different *n*-type partners such as ZnO,[13] CdS,[14,15] $Cd_{1-x}Zn_xS$,[16] SnS_2,[17] TiO_2,[18] and *a*-Si.[19] So far, the best SnS planar heterojunction device was fabricated with SnS/CdS, achieving a power conversion efficiency (η) of 1.3%.[14] The efficiencies achieved using heterojunctions of SnS with *n*-type materials other than CdS are extremely low (< 0.1%), mainly limited by low short-circuit current density (J_{sc} < 1.5 mA/cm^2). This poor J_{sc} is likely a result of bulk recombination in SnS because of defects, *e.g.*, grain boundaries, intrinsic point defects such as sulfur vacancies,[11] and/or impurities that arise from the preparation methods used to make the films.

In addition to the quality of SnS, other main contributors to this poor efficiency are believed to be an unfavorable conduction-band offset (CBO) and rapid carrier recombination at trap states near the interface between SnS and the *n*-type buffer layer. SnS/CdS forms a type-II heterojunction with the CBO ($\Delta E_c = \chi_{SnS} - \chi_{CdS}$, where χ is electron affinity) of –0.4 eV, which is an unfavorable band alignment for making efficient solar cells.[20] According to device simulations, a large negative CBO gives rise to an increase in the interface recombination, while a large positive CBO greater than +0.5 eV creates a barrier in the conduction band that impedes the collection of photo-generated electron.[21,22] Thus, a small positive CBO is desirable to reduce

interface recombination without any loss in photo-current collection.[21,22] One of the approaches to adjust the CBO is to vary the constituent elements in the semiconductor-alloy buffer layer. For example, (Zn,Cd)S,[23] (Zn,Mg)O,[24] (Zn,Sn)O_x,[25] and Zn(O,S)[26] were used in an attempt to replace CdS in CIGS solar cells. In this letter, we present a SnS device with a record power conversion efficiency of 2.04% (total area) using Zn(O,S) as an *n*-type buffer layer, and evaluate the effect of CBO on device performance.

A device structure of soda-lime glass/Mo/SnS/Zn(O,S)/ZnO/ITO was used in this study. SnS thin films were deposited on Mo-coated (450 nm) soda-lime glass substrates using a pulsed chemical vapor deposition (pulsed-CVD) process from the reaction of bis(*N*,*N'*-diisopropylacetamidinato)tin(II) (Sn(MeC(N-*i*Pr)$_2$)$_2$) and hydrogen sulfide (H_2S).[27] The sequence of one cycle of a pulsed-CVD is composed of (i) injection of tin precursor vapor using N_2 assistance, (ii) injection of H_2S gas to mix and react with the tin precursor vapor trapped inside the deposition zone for 1 s, and (iii) evacuation of the gas mixture and by-products for 2 s. Compared to a conventional atomic layer deposition (ALD) of SnS,[27] the pulsed-CVD process omits some purge steps, thereby increasing the deposition rate by more than an order of magnitude at the cost of some non-uniformity in the film thickness along the length of the reactor. The purity and optoelectrical properties of the obtained SnS films are the same as those grown from the ALD process reported elsewhere.[27] The substrate temperature was set to 200^{o}C. The tin precursor source was kept at 95°C. A gas mixture of 4% H_2S in N_2 (Airgas Inc.) was used as the source of sulfur. H_2S is a toxic, corrosive, and flammable gas (lower flammable limit of 4%).[28] Thus, it should be handled with caution. An appropriate reactor design for H_2S compatibility can be found elsewhere.[29] The partial pressures of tin precursor and H_2S after injecting into the deposition zone for each cycle are approximately 100 and 240 mTorr, respectively. Zn(O,S) (25-

30 nm) and ZnO (10 nm) were prepared by ALD at 120°C from the reaction of diethylzinc ($Zn(C_2H_5)_2$) (Sigma-Aldrich) with deionized water (H_2O) and hydrogen sulfide (H_2S). To ensure the quality of the interface, Zn(O,S) and ZnO layers were deposited immediately after the growth of SnS absorber layers without breaking vacuum. Indium tin oxide (ITO) (200 nm) was deposited at room temperature by RF magnetron sputtering through a shadow mask to define the cell area (0.031 or 0.71 cm^2). Additional electron-beam evaporated Al (500 nm) metal grids were used for the 0.71 cm^2 devices to further reduce the series resistance.

Device morphology was characterized using field-emission scanning electron microscopy (FESEM, Zeiss, Ultra-55). Rutherford backscattering spectrometry (RBS, Ionex 1.7 MV Tandetron) was performed to determine the elemental composition of Zn(O,S). The grain orientations of SnS films on Mo substrates were examined by X-ray diffraction (XRD, PANalytical X'Pert Pro) with Cu Kα radiation (λ = 1.542 Å) using θ-2θ scan. External quantum efficiency (EQE) measurements were made at room temperature, using a PV Measurements Model QEX7 tool. Transmittance (T) and reflectance (R) measurements were taken on a Hitachi U-4100 UV-Vis-NIR Spectrophotometer. Internal quantum efficiency (IQE) was calculated from IQE = EQE/(1-R). J-V measurements were made using a Keithley 2400 sourcemeter. The standard 1000 W/m^2 illumination was generated by a Newport Oriel 91194 solar simulator with a 1300 W Xe-lamp, an AM1.5G filter, and a Newport Oriel 68951 flux controller calibrated by an NREL-certified Si reference cell equipped with a BK-7 window. SunsV_{oc} measurements were made using a Suns-V_{oc}-150 Illumination Voltage Tester from Sinton Consulting Inc.[30]

To determine the optimum composition of the Zn(O,S) buffer layer for SnS, small devices with an active area of 0.031 cm^2 were fabricated using 500 nm-thick SnS with Zn(O,S) of different oxygen-to-sulfur ratios. By varying the cycle ratio of ZnO to ZnS during the ALD

process, the elemental composition of Zn(O,S) can be adjusted.[31] ZnO:ZnS cycle ratios of 4:1, 5.5:1 (which alternates 5:1 and 6:1), 6:1, and 7:1, which correspond to Zn(O,S) of O:S:Zn ratios = 0.42:0.73:1, 0.56:0.58:1, 0.64:0.50:1, and 0.72:0.37:1, respectively, were used to fabricate the devices. Figure 1 shows current density-voltage (*J-V*) characteristics under dark and illumination (~ 10 mW/cm^2) from a microscope halogen lamp (color temperature = 3300 K). This illumination condition, although different from the AM1.5 solar spectrum, is sufficient to test for junction character. Measured *J-V* characteristics suggest that for S/Zn > ~0.6, the SnS/Zn(O,S) junction exhibits type-I behavior with ΔE_c > +0.5 eV, *i.e.*, an energy barrier impedes photo-generated electron flow, resulting in a very low J_{sc}. For S/Zn ≤ ~0.5, the devices do not exhibit such a carrier collection problem and are thus believed to have ΔE_c < +0.5 eV. This trend corresponds well with the reported conduction band position of Zn(O,S), which is raised (lower χ) when the sulfur concentration in the film increases.[32]

After the optimum oxygen-to-sulfur ratios were determined for the Zn(O,S) buffer layer, larger-area devices (total area of 0.71 cm^2) were fabricated using 1.5 μm-thick SnS absorber layers with Zn(O,S) of S/Zn = 0.37 and 0.50. Figure 2 shows cross-sectional and plan-view SEM images of a device after Zn(O,S)/ZnO deposition. The SnS surface was covered uniformly by the buffer layer even at 25-30 nm thickness because of the conformal coating by ALD. The SnS film is columnar and composed of platelet-shaped grains. The observed cross-sectional grain size of SnS can be different (arrows in Fig. 2(a)) depending on the cleaving direction with respect to these platelet grains. Figure 3(a) displays *J-V* characteristics of these devices under dark and AM1.5 illumination. For S/Zn = 0.50, the device shows J_{sc} = 9.1 mA/cm^2, V_{oc} = 0.28 V, FF = 29.9%, and η = 0.74%. Surprisingly, unlike the 500 nm-SnS device (Fig. 1), the junction in this thicker SnS solar cell shows some signs of a large positive CBO including a dark/light *J-V* cross-

over, higher diode voltage (*i.e.* V_{oc}), small FF, and low J_{sc}.[33] This CBO discrepancy may be because of a variation of the SnS surface condition for different film thicknesses. Figure 3(b) shows the XRD spectra of SnS films grown on Mo layers as a function of SnS film thickness. The preferred crystal orientation of SnS film clearly shifts from (111) to (101) when the film thickness increases from 0.3 to 1.5 μm. Because of the anisotropic nature of the layered SnS compound,[11,34] such a change in crystallographic orientation can strongly affect the surface conduction-band position of SnS, and consequently its CBO with Zn(O,S).

The internal quantum efficiency (IQE) (Fig. 3(c), solid line) of the 1.5 μm-thick SnS devices with Zn(O,S) of S/Zn = 0.37 and 0.50 shows three distinct regions of carrier collection. Above 800 nm, the IQE is relatively low and limited by the low absorption coefficient and bulk recombination in SnS. The peaks of the IQE derivative (d(IQE)/dE) at 800 and 940 nm (1.55 and 1.32 eV, respectively) correspond well to the sharp rise in absorption coefficient of SnS[27] at these two wavelengths. Between 500 and 800 nm, compared to the S/Zn = 0.37 device, a significant drop in IQE of the S/Zn = 0.50 device is observed because of the large positive CBO. Below 500 nm, the S/Zn = 0.50 composition provides a better carrier collection despite having the large conduction-band energy barrier. This improved IQE at smaller wavelength can happen from photo-doping in the buffer layer, which results in a downward shift in the conduction band and thus reduces the CBO barrier.[35] In addition, Zn(O,S) of S/Zn = 0.50 also has a lower absorption tail as shown in Fig. 3(d) and thus exhibits a better blue response.

The S/Zn = 0.37 device (Fig. 3(a)) exhibits the best performance with J_{sc} = 16.8 mA/cm^2, V_{oc} = 0.22 V, FF = 47.7%, and η = 1.8%. The same device was characterized independently at the National Renewable Energy Laboratory (NREL), exhibiting an improved cell performance of J_{sc} = 19.4 mA/cm^2, V_{oc} = 0.244 V, FF = 42.97%, and η = 2.04%, as shown in Fig. 4. We suspect

that the discrepancy between NREL and our in-house measurements arises from lower illumination of our solar simulator. This device shows the highest recorded and independently verified efficiency of a planar SnS-based solar cell to date. This result demonstrates the flexibility of Zn(O,S) as an adjustable-CBO buffer layer for different surfaces or materials, which cannot be achieved in binary compounds (*e.g.,* CdS, ZnO, ZnS, TiO_2, or In_2S_3). The short-circuit current density of 19.4 mA/cm^2 is significantly higher than all previously reported SnS solar cells (9.6 mA/cm^2). This result is probably because of a better interface junction with Zn(O,S) and/or fewer defects in our SnS films, compared to other previously reported deposition techniques. The minority-carrier collection length (defined as depletion width + minority-carrier diffusion length) is roughly estimated from the IQE data of S/Zn = 0.37 device fitted with a combined space-charge and minority-carrier diffusion length collection model (IQE $\cong$ 1 – [exp(–$\alpha \times W$)]/[$\alpha \times L$ + 1]), where α is the optical absorption coefficient, L is the minority-carrier diffusion length and W is the width of the depletion region), primarily used for absorbers such as CIGS and CdTe.[36] The fit suggests a minority-carrier collection length range of 0.2-0.4 μm. For further improvement, a heat treatment of SnS may be required to increase the grain size and reduce defects in the material.

It is worthwhile to note that additional improvements of FF can be made on current devices by optimizing the device structure alone; the Al metal grid used in these devices was too thin (500 nm), and the series resistance (estimated to be 6.0 Ω·cm^2 from fitted *J-V* curves) notably reduced the FF of the device. Using SunsV_{oc}[30,37] (data not shown), the FF without the effect of series resistance is estimated to be 60%. This improvement in FF alone would yield a device with a pseudo-efficiency of 2.9%. In addition, the metal contact grid also covered 17% of the total cell area and created a significant shadowing loss. Adjusting the NREL-certified

efficiency for this shadowing loss, the active-area efficiency is estimated to be 2.46%. The addition of an antireflection coating should help reduce the reflectance loss (~15% from reflectance measurements). Lastly, lock-in thermography images (not shown) indicate a noticeable leakage current around the perimeter of the device, a likely consequence of the lack of edge isolation.

In conclusion, a SnS-based device (total area of 0.71 cm^2) comprising a Zn(O,S) buffer layer achieved an NREL-certified full-area solar cell efficiency of 2.04%, and an uncertified active-area efficiency of 2.46%. The SnS absorber layer was deposited via pulsed-CVD, followed by ALD of the buffer layer without breaking vacuum. The optimum oxygen-to-sulfur ratio was found to vary depending on the absorber layer thickness (*i.e.*, SnS preferred grain orientation), between S/Zn = 0.50 and 0.37 for 500 nm and 1.5 μm, respectively. The versatility of Zn(O,S) for CBO tuning was demonstrated, which could be utilized for a systematic study in other absorber materials as well. We expect that efficiencies can be further improved by optimizing contact geometry (shading losses, series resistance), adding an antireflection coating, improving bulk minority carrier diffusion length, reducing absorber thickness, and eliminating edge shunting; efficiencies can be improved by an order of magnitude or more, considering the Shockley-Queisser efficiency limit for SnS of 32%.

Acknowledgements

We thank S. R. Kurtz, P. Ciszek, and the NREL cell measurement team for assistance with certified cell testing; J.T. Sullivan (MIT) with lock-in thermography measurements; J.T. Sullivan and R.E. Brandt (MIT) for helpful discussions; and M. Sher (Harvard University) with reflectivity measurements. The experimental contributions of Y. Segal in the early stages of this

work are acknowledged. This work was supported by the U. S. National Science Foundation under NSF Award No. CBET-1032955, the U.S. Department of Energy SunShot Initiative under Contract No. DE-EE0005329, and by Saint Gobain S. A. which also supplied Mo-coated glass slides. P. Sinsermsuksakul acknowledges support from the Development and Promotion of Science and Technology Talents Project (DPST), Thailand. K. Hartman acknowledges the support of a National Science Foundation Graduate Research Fellowship. This work was performed in part at Harvard University's Center for Nanoscale Systems (CNS), a member of the National Nanotechnology Infrastructure Network (NNIN), which is supported by the National Science Foundation under NSF award No. ECS-0335765.

Reference

[1] C. Wadia, A. P. Alivisatos, and D. M. Kammen, Environ. Sci. Technol. **43** (6), 2072-2077 (2009).
[2] A. Mittiga, E. Salza, F. Sarto, M. Tucci, and R. Vasanthi, Appl. Phys. Lett. **88** (16), 163502 (2006).
[3] Y. Wu, C. Wadia, W. L. Ma, B. Sadtler, and A. P. Alivisatos, Nano Lett. **8** (8), 2551-2555 (2008).
[4] J. Puthussery, S. Seefeld, N. Berry M. Gibbs, and M. Law, J. Am. Chem. Soc. **133** (4), 716-719 (2011).
[5] N. Berry, M. Cheng, C.L. Perkins, M. Limpinsel, J. C. Hemminger, and M. Law, Adv. Energy Mater. **2** (9), 1124-1135 (2012).
[6] D. B. Mitzi, O. Gunawan, T. K. Todorov, K. Wang, and S. Guha, Sol. Energ. Mat. Sol. C **95** (6), 1421-1436 (2011).
[7] D. O. Scanlon and A. Walsh, Appl. Phys. Lett. **100** (25), 251911 (2012).
[8] K. Hartman, J. L. Johnson, M. I. Bertoni D. Recht, M. J. Aziz, M. A. Scarpulla, and T. Buonassisi, Thin Solid Films **519** (21), 7421-7424 (2011).
[9] M. Devika, N. K. Reddy, K. Ramesh, R. Ganesan, K. R. Gunasekhar, E. S. R. Gopal, and K. T. R. Reddy, J. Electrochem. Soc. **154** (2), H67-H73 (2007).
[10] N. K. Reddy, Y. B. Hahn, M. Devika, H. R. Sumana, and K. R. Gunasekhar, J. Appl. Phys. **101** (9), 093522 (2007).
[11] J. Vidal, S. Lany, M. d'Avezac, A. Zunger, A. Zakutayev, J. Francis, and J. Tate, Appl. Phys. Lett. **100** (3), 032104 (2012).
[12] G. Yue, Y. Lin, X. Wen, L. Wang, and D. Peng, J. Mater. Chem. **22** (32), 16437-16441 (2012).
[13] B. Ghosh, M. Das, P. Banerjee, and S. Das, Semicond. Sci. Tech. **24** (2), 025024 (2009).

[14] K. T. R. Reddy, N. K. Reddy, and R. W. Miles, Sol. Energ. Mat. Sol. C **90** (18-19), 3041-3046 (2006).
[15] S. A. Bashkirov, V. F. Gremenok, V. A. Ivanov, V. V. Lazenka, and K. Bente, Thin Solid Films **520** (17), 5807-5810 (2012).
[16] M. Gunasekaran and M. Ichimura, Sol. Energ. Mat. Sol. C **91** (9), 774-778 (2007).
[17] A. Sanchez-Juarez, A. Tiburcio-Silver, and A. Ortiz, Thin Solid Films **480**, 452-456 (2005).
[18] Y. Wang, H. Gong, B. H. Fan, and G. X. Hu, J. Phys. Chem. C **114** (7), 3256-3259 (2010).
[19] F. Jiang, H. L. Shen, W. Wang, and L. Zhang, J. Electrochem. Soc. **159** (3), H235-H238 (2012).
[20] M. Sugiyama, K. T. R. Reddy, N. Revathi, Y. Shimamoto, and Y. Murata, Thin Solid Films **519** (21), 7429-7431 (2011).
[21] A. Niemegeers, M. Burgelman, and A. Devos, Appl. Phys. Lett. **67** (6), 843-845 (1995).
[22] T. Minemoto, T. Matsui, H. Takakura, Y. Hamakawa, T. Negami, Y. Hashimoto, T. Uenoyama, and M. Kitagawa, Sol. Energ. Mat. Sol. C **67** (1-4), 83-88 (2001).
[23] B. Kumar, P. Vasekar, S. A. Pethe, N. G. Dhere, and G. I. Koishiyev, Thin Solid Films **517** (7), 2295-2299 (2009).
[24] T. Minemoto, Y. Hashimoto, T. Satoh, T. Negami, H. Takakura, and Y. Hamakawa, J. Appl. Phys. **89** (12), 8327-8330 (2001).
[25] M. Kapilashrami, C. X. Kronawitter, T. Torndahl, J. Lindahl, A. Hultqvist, W. C. Wang, C. L. Chang, S. S. Mao, and J. H. Guo, Phys. Chem. Chem. Phys. **14** (29), 10154-10159 (2012).
[26] C. Platzer-Bjorkman, T. Torndahl, D. Abou-Ras, J. Malmstrom, J. Kessler, and L. Stolt, J. Appl. Phys. **100** (4), 044506 (2006).
[27] P. Sinsermsuksakul, J. Heo, W. Noh, A. S. Hock, and R. G. Gordon, Adv. Energy Mater. **1** (6), 1116-1125 (2011).
[28] *Hydrogen Sulfide*; MSDS No.001029; Airgas Inc.: Radnor, PA. April 26, (2010).
[29] N. P. Dasgupta, J. F. Mack, M. C. Langston, A. Bousetta, and F. B. Prinz, Rev. Sci. Instrum. **81** (4), 044102 (2010).
[30] R. A. Sinton and A. Cuevas, Proc. 16th European Photovoltaic Solar Energy Conf. 1152-1155 (UK, 2000).
[31] B. W. Sanders and A. Kitai, Chem. Mater. **4** (5), 1005-1011 (1992).
[32] C. Persson, C. Platzer-Bjorkman, J. Malmstrom, T. Torndahl, and M. Edoff, Phys. Rev. Lett. **97** (14), 146403 (2006).
[33] A. O. Pudov, A. Kanevce, H. A. Al-Thani, J. R. Sites, and F. S. Hasoon, J. Appl. Phys. **97** (6), 064901 (2005).
[34] W. Albers, H. J. Vink, C. Haas, and J. D. Wasscher, J. Appl. Phys. **32**, 2220-2225 (1961).
[35] A. O. Pudov, J. R. Sites, M. A. Contreras, T. Nakada, and H. W. Schock, Thin Solid Films **480**, 273-278 (2005).
[36] S.S. Hegedus and W.N. Shafarman, Prog. Photovolt: Res. Appl. **12**, 155-176 (2004).
[37] M. J. Kerr and A. Cuevas, Sol. Energy **76** (1-3), 263-267 (2004).

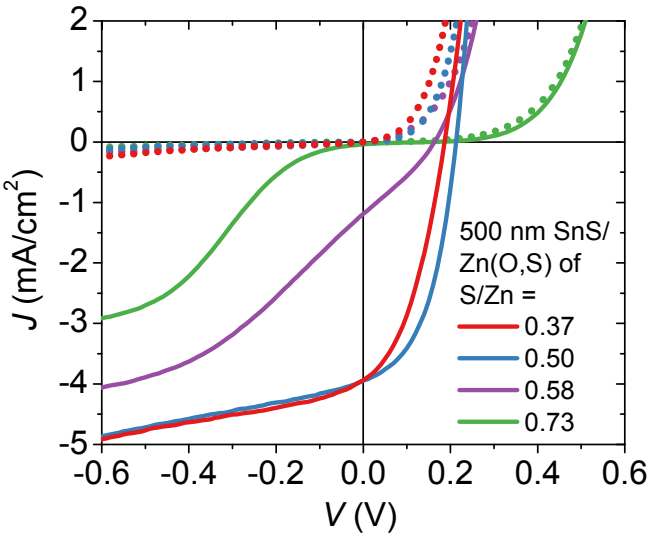

FIG. 1. Current density-voltage characteristics of Mo/500 nm-SnS/Zn(O,S)/ZnO/ITO devices at different Zn(O,S) compositions ($0.35 < S/Zn < 0.75$) under dark (dotted line) and ~10 mW/cm^2 illumination (solid line).

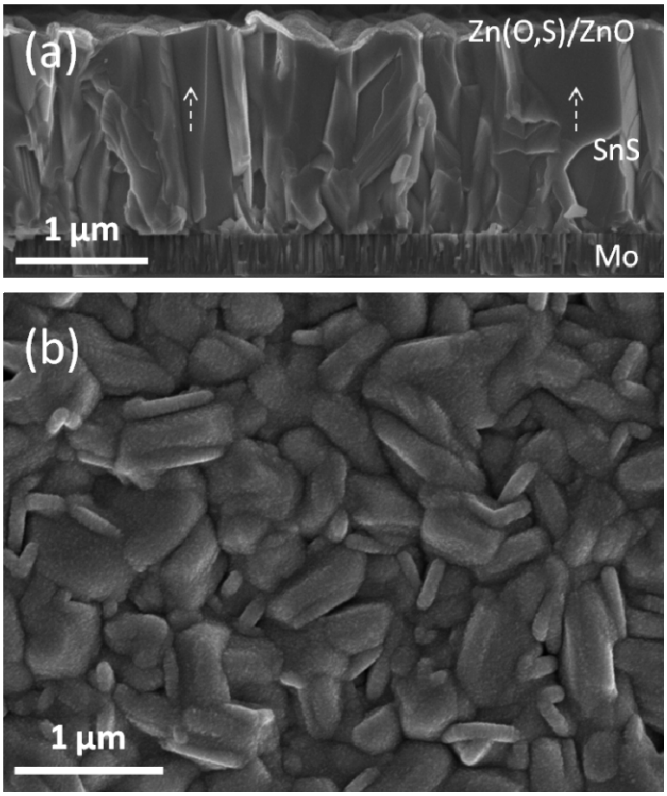

FIG. 2. SEM images of **(a)** cross-sectional and **(b)** plan-view of Mo/SnS/Zn(O,S)/ZnO before top contact fabrication, showing a dense and conformal coverage of the Zn(O,S) and ZnO layers grown via ALD.

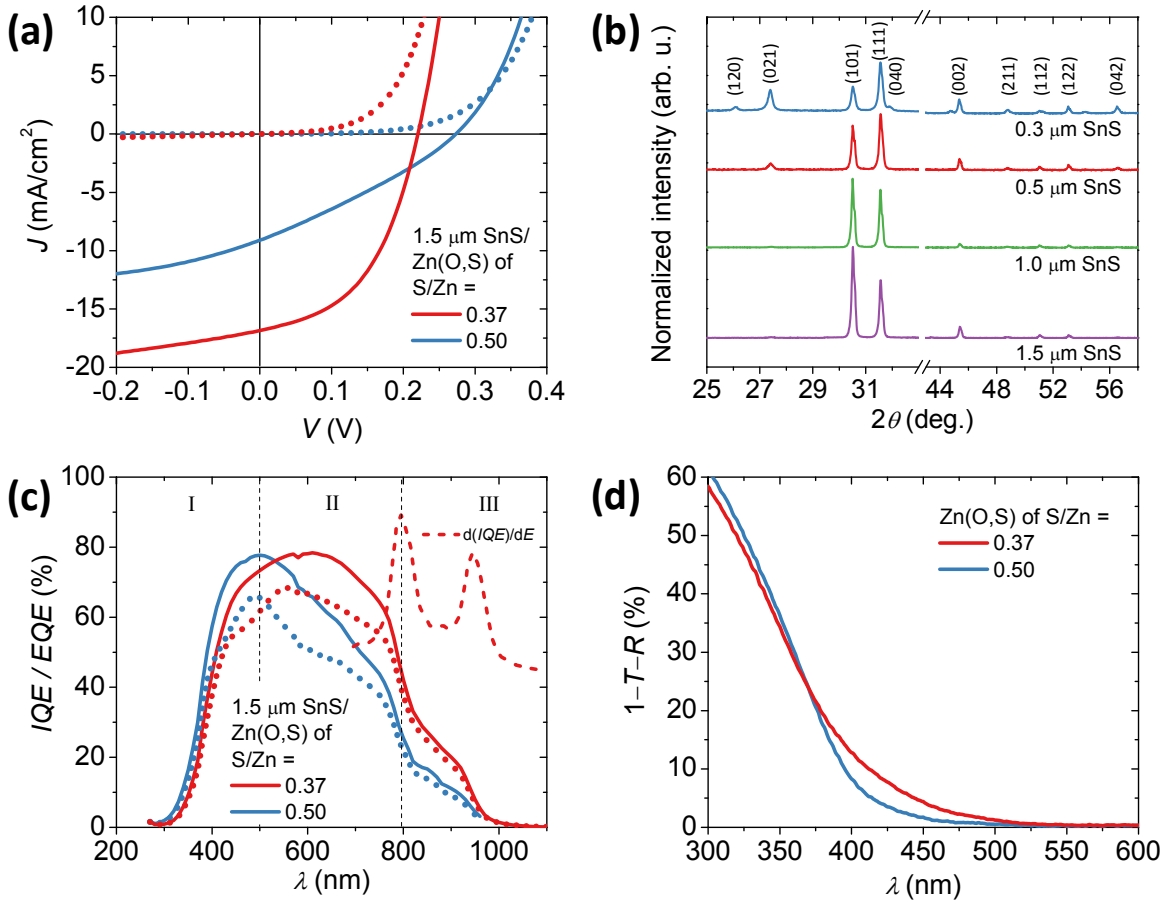

FIG. 3. (a) *J*-*V* characteristic of 1.5 μm-thick SnS devices with Zn(O,S) of S/Zn = 0.37 and 0.50 under dark (dotted line) and approximately 1 sun illumination (solid line). (b) XRD spectra of SnS at the film thicknesses of 0.3, 0.5, 1.0, and 1.5 μm. The intensity was normalized by the (111) peak. (c) IQE (solid line) and EQE (dotted line) of the same devices. The peaks of the IQE derivatives in the S/Zn = 0.37 device correspond to the strong absorption edges of SnS at 1.32 and 1.55 eV. (d) Effective absorption (1-*T*-*R*) of 60 nm-thick Zn(O,S) of S/Zn = 0.37 and 0.50.

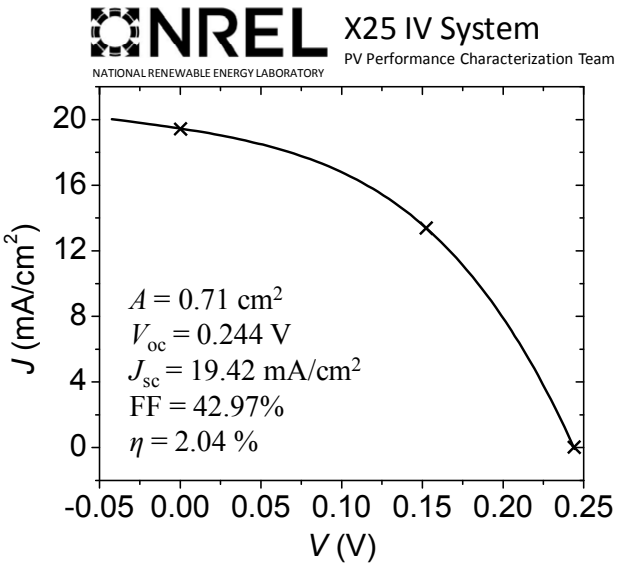

FIG. 4. A champion SnS/Zn(O,S) solar cell with a record efficiency of 2.04% (total area), as certified by NREL.